Supplementary Materials:

Jianping Duan [1,*], Peili Wu [2] and Zhuguo Ma [1,3]

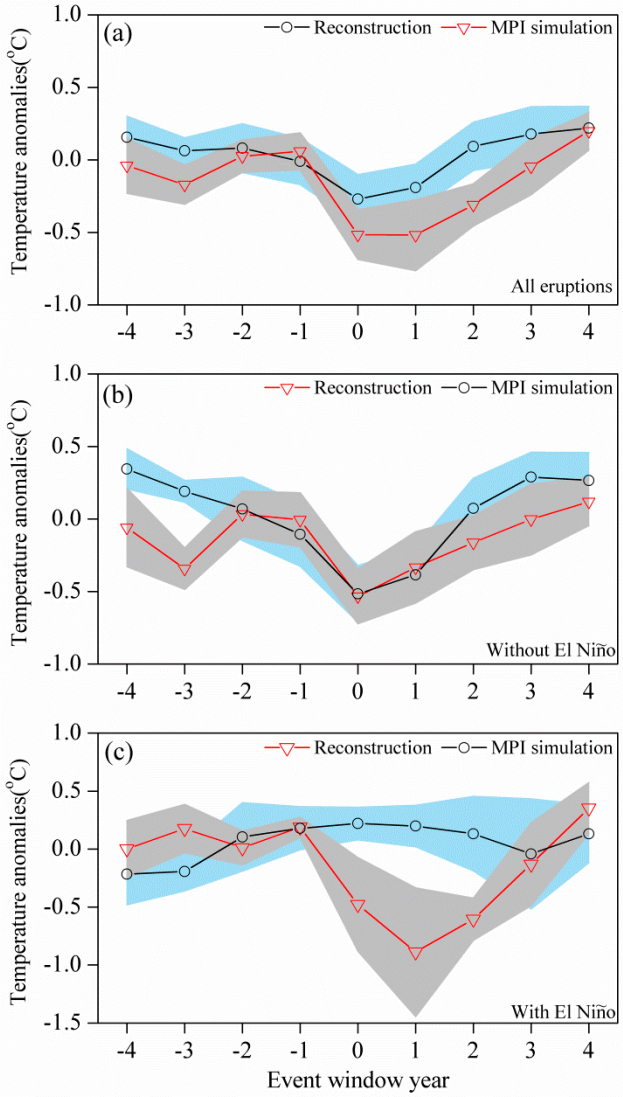

Figure S1. Comparisons between the composite magnitudes of post-volcanic August-September cooling over the TP derived from the tree-ring density-based reconstruction and simulation from MPI model. The composite magnitude was based on (**a**) all the twelve large tropical eruptions, (**b**) the eight large tropical eruptions without El Niño associations and (**c**) the four large tropical eruptions accompanied by a subsequent El Niño event. Temperature anomalies in (**a-c**) are with respect to the preceding 5-year mean. The shaded areas denote the error bar (SE).

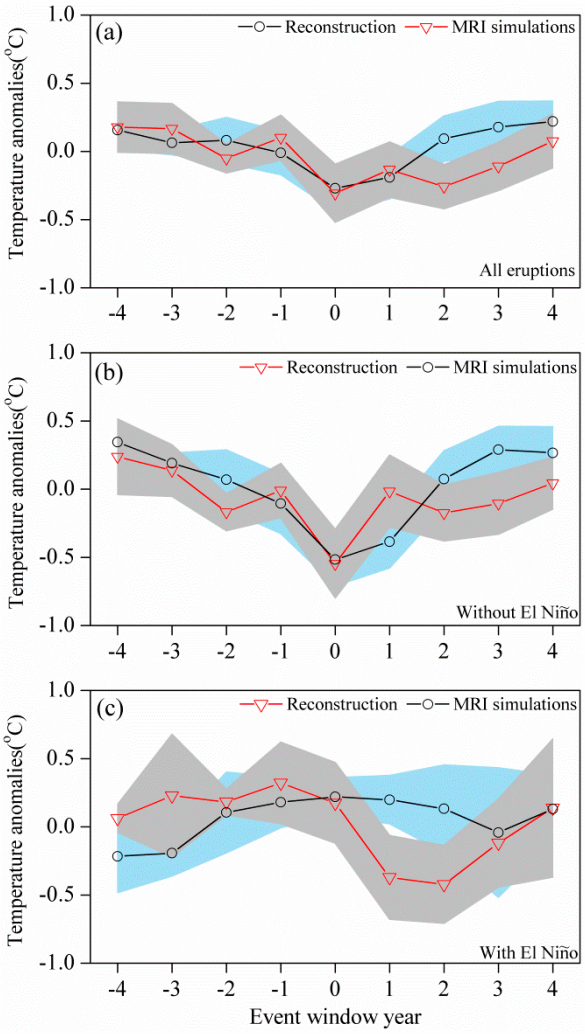

Figure S2. Comparisons between the composite magnitudes of post-volcanic August-September cooling over the TP derived from the tree-ring density-based reconstruction and simulation from MRI model. The composite magnitude was based on (**a**) all the twelve large tropical eruptions, (**b**) the eight large tropical eruptions without El Niño associations and (**c**) the four large tropical eruptions accompanied by a subsequent El Niño event. Temperature anomalies in (**a-c**) are with respect to the preceding 5-year mean. The shaded areas denote the error bar (SE).

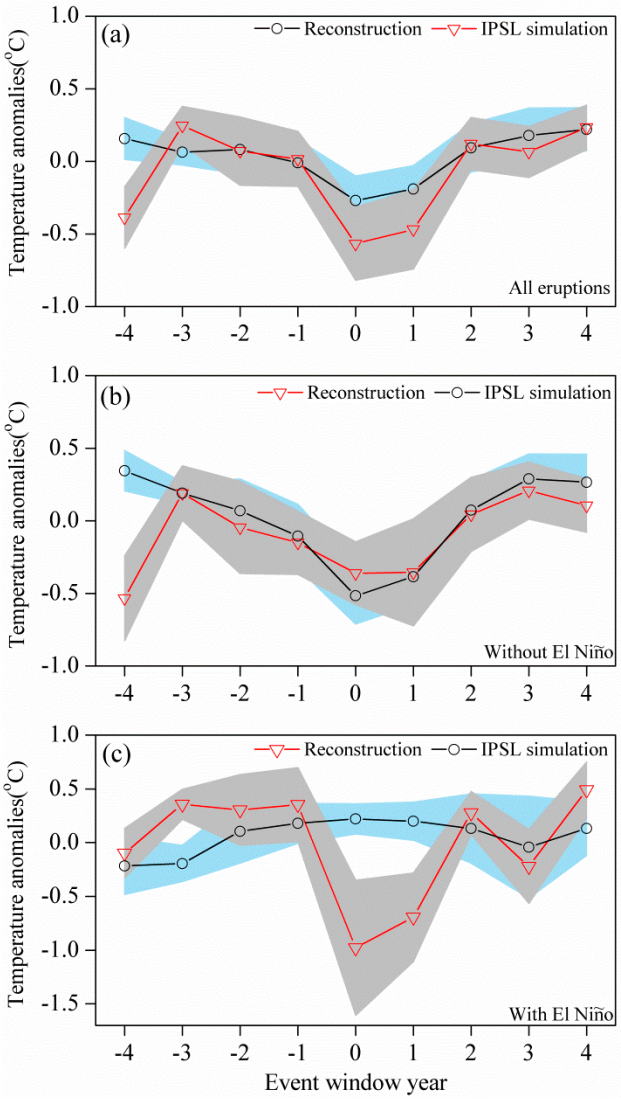

Figure S3. Comparisons between the composite magnitudes of post-volcanic August-September cooling over the TP derived from the tree-ring density-based reconstruction and simulation from IPSL model. The composite magnitude was based on (**a**) all the twelve large tropical eruptions, (**b**) the eight large tropical eruptions without El Niño associations and (**c**) the four large tropical eruptions accompanied by a subsequent El Niño event. Temperature anomalies in (**a-c**) are with respect to the preceding 5-year mean. The shaded areas denote the error bar (SE).

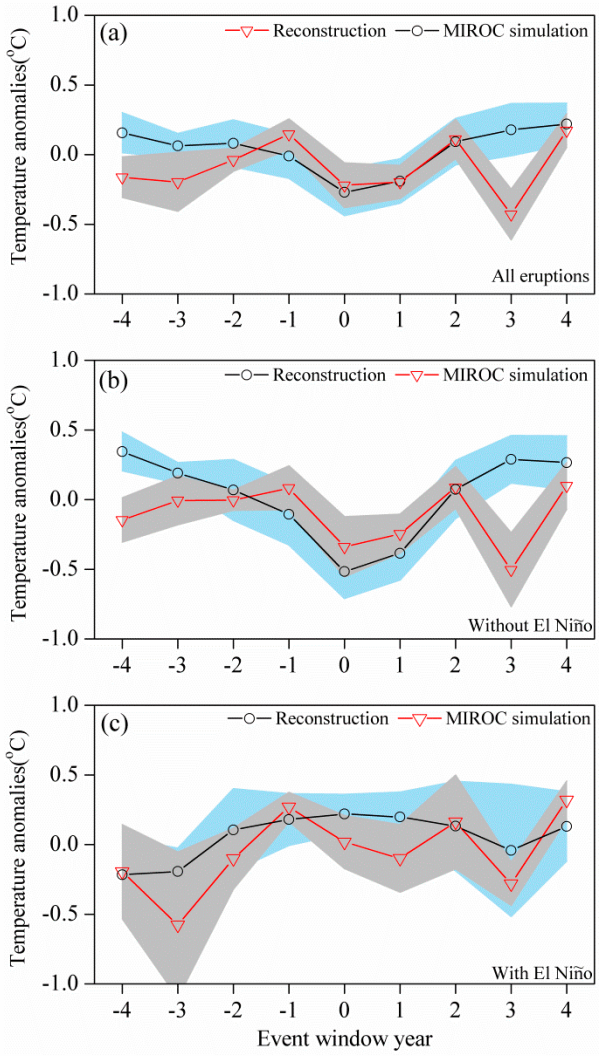

Figure S4. Comparisons between the composite magnitudes of post-volcanic August-September cooling over the TP derived from the tree-ring density-based reconstruction and simulation from MIROC model. The composite magnitude was based on (**a**) all the twelve large tropical eruptions, (**b**) the eight large tropical eruptions without El Niño associations and (**c**) the four large tropical eruptions accompanied by a subsequent El Niño event. Temperature anomalies in (**a-c**) are with respect to the preceding 5-year mean. The shaded areas denote the error bar (SE).

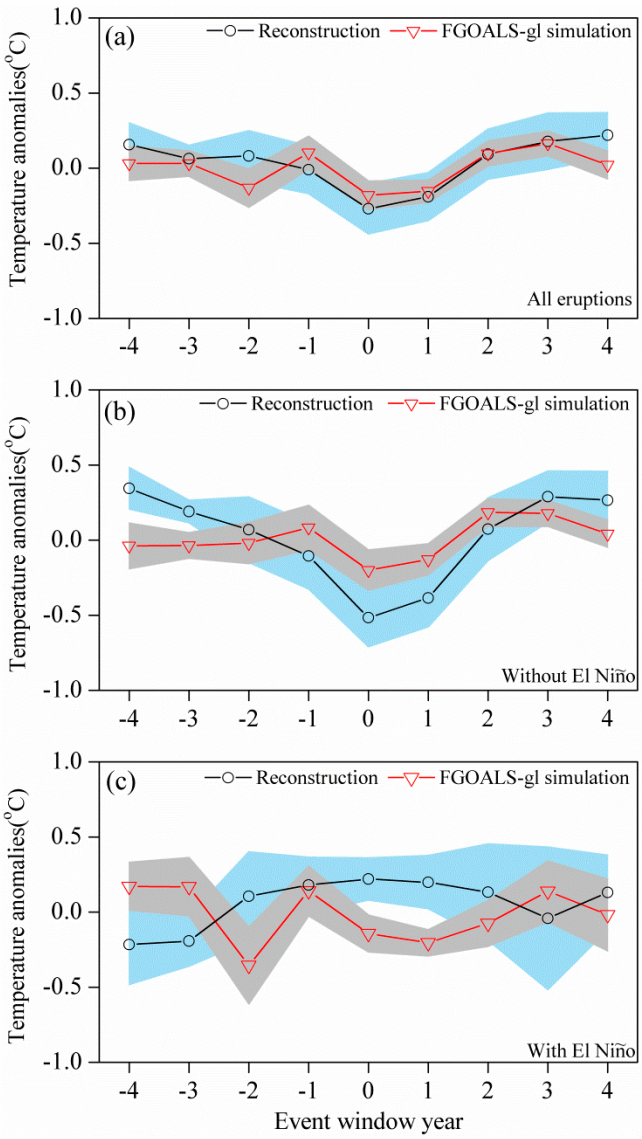

Figure S5. Comparisons between the composite magnitudes of post-volcanic August-September cooling over the TP derived from the tree-ring density-based reconstruction and simulation from FGOALS-gl model. The composite magnitude was based on (**a**) all the twelve large tropical eruptions, (**b**) the eight large tropical eruptions without El Niño associations and (**c**) the four large tropical eruptions accompanied by a subsequent El Niño event. Temperature anomalies in (**a-c**) are with respect to the preceding 5-year mean. The shaded areas denote the error bar (SE).

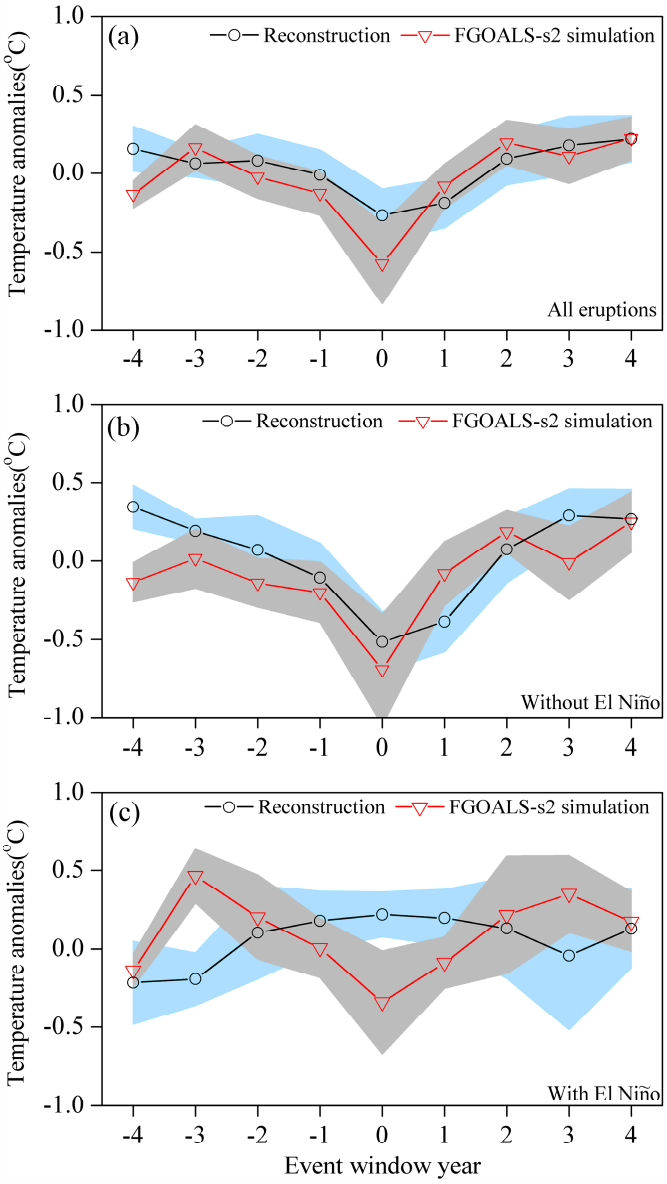

Figure S6. Comparisons between the composite magnitudes of post-volcanic August-September cooling over the TP derived from the tree-ring density-based reconstruction and simulation from FGOALS-s2 model. The composite magnitude was based on (**a**) all the twelve large tropical eruptions, (**b**) the eight large tropical eruptions without El Niño associations and (**c**) the four large tropical eruptions accompanied by a subsequent El Niño event. Temperature anomalies in (**a-c**) are with respect to the preceding 5-year mean. The shaded areas denote the error bar (SE).

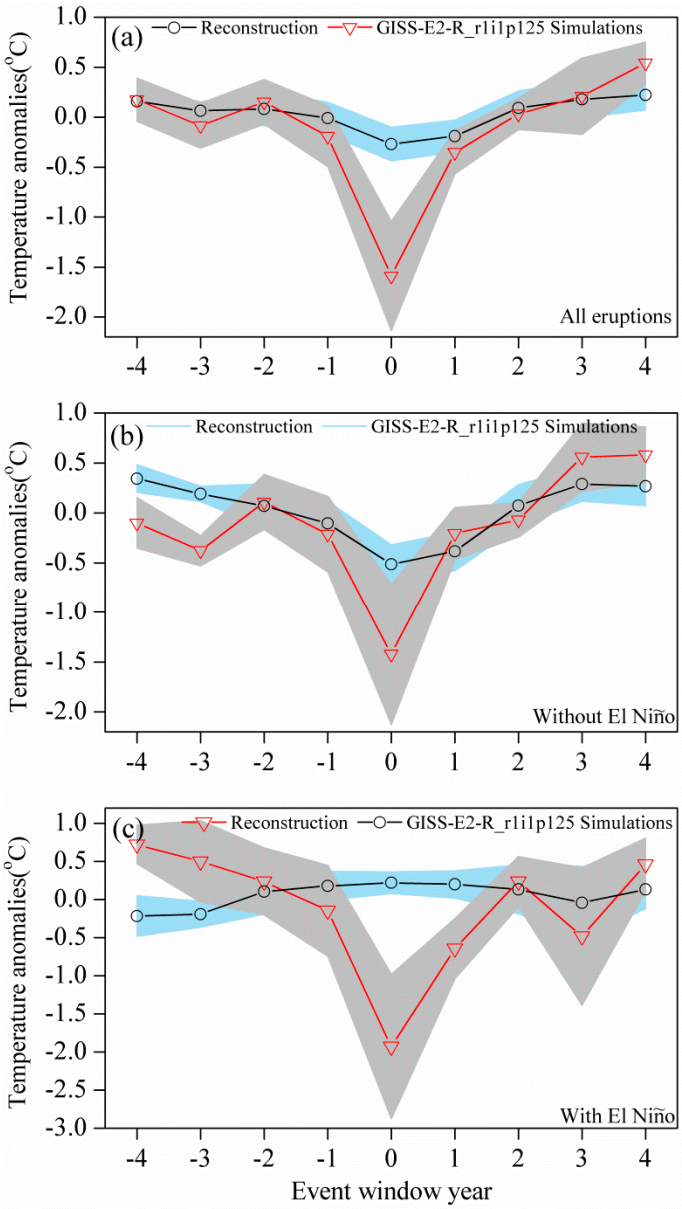

Figure S7. Comparisons between the composite magnitudes of post-volcanic August-September cooling over the TP derived from the tree-ring density-based reconstruction and simulation from GISS-E2-R-r1i1p125 model. The composite magnitude was based on (**a**) all the twelve large tropical eruptions, (**b**) the eight large tropical eruptions without El Niño associations and (**c**) the four large tropical eruptions accompanied by a subsequent El Niño event. Temperature anomalies in (**a-c**) are with respect to the preceding 5-year mean. The shaded areas denote the error bar (SE).

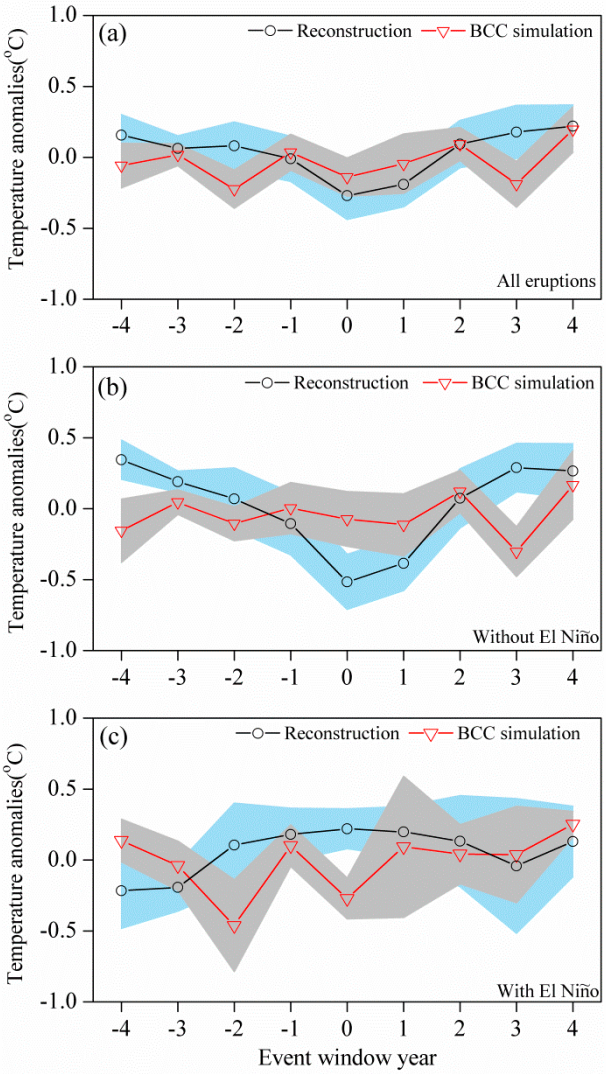

Figure S8. Comparisons between the composite magnitudes of post-volcanic August-September cooling over the TP derived from the tree-ring density-based reconstruction and simulation from BCC-CSM1.1 model. The composite magnitude was based on (**a**) all the twelve large tropical eruptions, (**b**) the eight large tropical eruptions without El Niño associations and (**c**) the four large tropical eruptions accompanied by a subsequent El Niño event. Temperature anomalies in (**a-c**) are with respect to the preceding 5-year mean. The shaded areas denote the error bar (SE).

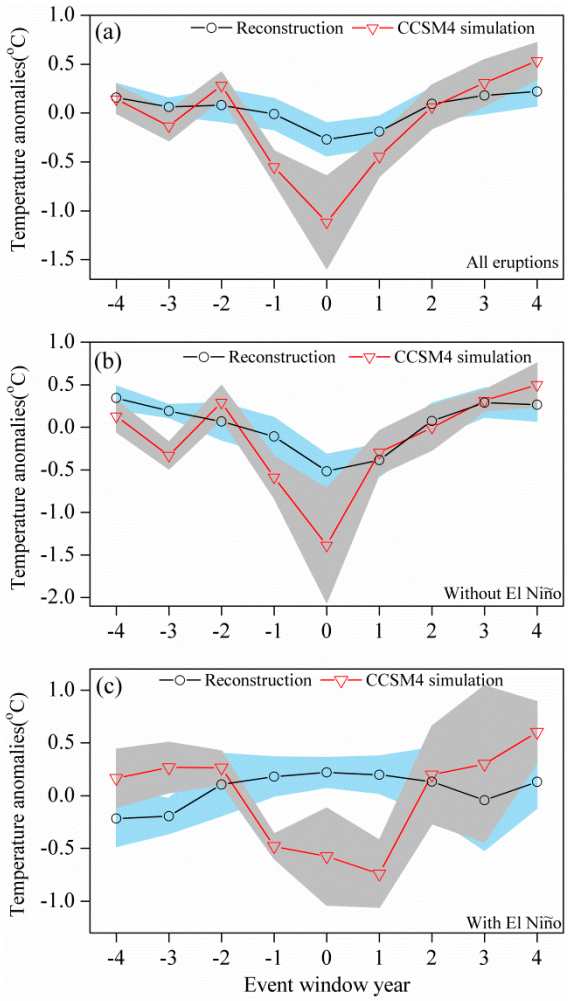

Figure S9. Comparisons between the composite magnitudes of post-volcanic August-September cooling over the TP derived from the tree-ring density-based reconstruction and simulation from CCSM4 model. The composite magnitude was based on (**a**) all the twelve large tropical eruptions, (**b**) the eight large tropical eruptions without El Niño associations and (**c**) the four large tropical eruptions accompanied by a subsequent El Niño event. Temperature anomalies in (**a-c**) are with respect to the preceding 5-year mean. The shaded areas denote the error bar (SE).